



## Removal of pollutants by the new Fenton-like highly active catalysts containing an imidazolium salt and a Schiff base



M. Neamțu<sup>a,\*</sup>, F. Macaev<sup>b</sup>, V. Boldescu<sup>b</sup>, V.-D. Hodoroaba<sup>c</sup>, C. Nădejde<sup>a</sup>, R.J. Schneider<sup>c</sup>, A. Paul<sup>c</sup>, G. Ababei<sup>d</sup>, U. Panne<sup>c,e</sup>

<sup>a</sup> Interdisciplinary Research Department—Field Science, ‘Alexandru Ioan Cuza’ University, Iascani Catargi Str. 54, 700107 Iasi, Romania

<sup>b</sup> Laboratory of organic synthesis, Institute of Chemistry, Academy of Sciences of Moldova, Academy Str. 3, MD-2028 Chisinau, Republic of Moldova

<sup>c</sup> BAM Federal Institute for Materials Research and Testing, Unter den Eichen 87, 12205 Berlin, Germany

<sup>d</sup> National Institute of Research and Development for Technical Physics, Dimitrie Mangeron Bd. 47, 700050 Iasi, Romania

<sup>e</sup> Humboldt-Universität zu Berlin, Department of Chemistry, Brook-Taylor-Str. 2, 12489 Berlin, Germany

### ARTICLE INFO

#### Article history:

Received 24 August 2015

Received in revised form 1 October 2015

Accepted 14 October 2015

Available online 30 October 2015

#### Keywords:

Fe-based highly active ionic liquids  
Characterization of catalysts  
Removal of carbamazepine  
Singlet oxygen

### ABSTRACT

Two iron-based molten salts comprising an imidazolium and Schiff base were evaluated as catalysts for removal of carbamazepine (CBZ) from water. The catalysts were fully characterized using scanning electron microscopy (SEM), energy-dispersive X-ray spectrometry (EDX), nuclear magnetic resonance spectroscopy (NMR), electrospray ionisation–mass spectrometry (ESI–MS), differential scanning calorimetry (DSC), Fourier transform infrared spectroscopy (FTIR) and nitrogen adsorption–desorption isotherms (BET). Additionally, the formation of photo-sensitized oxygen was investigated by spin-trapping using electron spin resonance (ESR). The catalytic activity in heterogeneous oxidation of the micropollutant (CBZ) was also evaluated. The effects of catalyst loading, pH, H<sub>2</sub>O<sub>2</sub> dosage and UV light on the oxidation of the selected compound were investigated. After 15 min of UVA irradiation in the presence of 200 μM H<sub>2</sub>O<sub>2</sub>, CBZ was completely removed over both catalysts.

© 2015 Elsevier B.V. All rights reserved.

### 1. Introduction

Pharmaceuticals are a large and diverse group of compounds used in very high amounts. The presence of a large variety of pharmaceuticals in concentrations of ng/L to μg/L in effluents of sewage treatment plants, river, surface and ground waters as well as in drinking water [1–6] has been reported. Even at low concentration they may still have the potential to cause chronic effects [7]. Although the individual environmental concentrations of the pharmaceuticals are very low, effects of their mixture on living organisms are unknown and, therefore, unpredictable [8].

Carbamazepine (CBZ), an antiepileptic drug, is one of the most commonly detected pharmaceutical drugs in the aquatic environment [9]. Due to its widespread occurrence, low efficiencies of the removal (below 10%) in wastewater treatment process and environmental persistence it is used as an anthropogenic marker of urban pollution [10]. It has been proven that even at concentrations found in environment, CBZ can affect biochemical pathways of the living organisms [11–14].

On the other hand, another study has demonstrated that a simple UV treatment of CBZ containing solutions leads to formation of even more toxic degradation products: acridine and acridone [15]. The importance of usage of different catalysts in complete photodegradation of CBZ has been shown by Haroune et al. [16]. It is well known that most cost-effective technologies to treat wastewaters polluted with micropollutants are the processes using Fenton-like nanocatalysts [17,18].

Ionic liquids (ILs) have long been known to possess many useful properties and have a high potential for application as an alternative to classic solvents [19], electrolytes in batteries and fuel cells [20,21], and lubricants [22]. The most important properties that make the ILs so attractive include their ability to dissolve a wide range of inorganic and organic compounds, and their high polarity, low volatility and, as a result, low flammability. Exploitation of these properties led to a widespread use of ionic liquids in chemical synthesis for extraction, separation and catalysis [23]. In the last decades functionalized ILs containing metals such as Fe(II), Fe(III), Zn(II) and Al(III) have been attracting rising interest in both homogeneous and heterogeneous catalysis. For the environmental application ILs have a great potential in extraction of metal ions from polluted industrial and communal waters [24], fuel desulfu-

\* Corresponding author. Fax: +40 232 201 102.

E-mail address: [mariana.neamtu@uaic.ro](mailto:mariana.neamtu@uaic.ro) (M. Neamțu).

rization [25,26], and removal of dioxins from exhaust gases and vapors [27].

For specific purposes, so-called “task-specific” ionic liquids (TSILs) can be obtained. In particular, transition metal-containing ionic liquids, with the IL as a ligand, can be applied in the catalysis of many organic transformations. In comparison with traditional ligand-supported systems, transition metal-containing ionic liquids (or so-called ionic transition metal complexes) can offer certain “green” advantages such as stability, efficiency, low toxicity, and reusability [28]. Since iron is one of the most inexpensive and non-pollutant metals, the use of iron-containing ionic liquids in variable organic reactions is of great interest and constantly growing. In this paper we describe synthesis and use of a novel imidazolium-based iron-containing ionic substance and its paramagnetic form via a Fenton-like process in the treatment of wastewaters polluted with CBZ. We present the characterization and application of two catalysts. Additionally, the formation of photo-sensitized oxygen by spin-trapping using electron spin resonance (ESR) has been investigated.

## 2. Experimental

### 2.1. Reagents

The chemicals used were of reagent grade and used as received. The high-purity CBZ and 2,2,6,6-tetramethyl-4-piperidinol were purchased from Sigma–Aldrich (Germany). Solvents were of HPLC quality. Water for HPLC–MS/MS was ultrapure (MilliQ, Millipore). Hydrogen-peroxide solution (30%, Sigma–Aldrich) and all chemicals used for solutions (such as buffer, eluents) were reagent grade and used without further purification. Removal of all solvents was carried out under reduced pressure.

### 2.2. Synthesis of the catalysts

#### 2.2.1. Synthesis of 5-(chloromethyl)-2-hydroxybenzaldehyde (2)

10.00 g (82 mmol) of salicylic aldehyde (1) were added dropwise under stirring to the solution of 7.50 g paraformaldehyde in 150 mL of HCl (conc.). The mixture was subjected to stirring during 24 h at room temperature. The formed precipitate was filtered, washed with water, dissolved in diethyl ether after which it was dried and evaporated. The obtained product then was subjected to recrystallization from hexane to give white solid product. The reaction yield was 60%. M.p. = 87.5 °C. IR  $\nu$ ,  $\text{cm}^{-1}$ : 3220, 3044, 2966, 2966, 2878, 2753, 1953, 1722, 1649, 1621, 1579, 1474, 1381, 1309, 1281, 1257, 1241, 1188, 1147, 1116, 1009, 948, 914, 903, 849, 798, 768, 720, 687, 670. Elemental composition: formula  $\text{C}_8\text{H}_7\text{ClO}_2$ . Calculated, %: C 56.32, H 4.14, found, %: C 56.41, H 4.10.

For recent example of synthesis of (2) see [29].

#### 2.2.2. Synthesis of

3-(3-formyl-4-hydroxybenzyl)-1-methyl-1H-imidazol-3-ium chloride (4)

1.50 g (9 mmol) of 5-(chloromethyl)-2-hydroxybenzaldehyde (2) was dissolved in 10 mL of acetonitrile. Then, 0.73 g (9 mmol) of 1-methylimidazol (3) were added dropwise to the acetonitrile solution while stirring. The mixture was refluxed at stirring for 6 h. The reaction was controlled by thin-layer chromatography (TLC). The product was filtered and washed with hexane and diethyl ether, and then it was dried at RT to give pale yellow solid product. The reaction yield was 85%. M.p. = 192–195 °C. IR  $\nu$ ,  $\text{cm}^{-1}$ : 3661, 3457, 3400, 3250, 3148, 3085, 3050, 2989, 2943, 2888, 2793, 2699, 2554, 2466, 2041, 1915, 1761, 1677, 1616, 1576, 1562, 1500, 1439, 1427, 1353, 1291, 1243, 1197, 1172, 1145, 1110, 1089, 1028, 965, 951, 875, 831, 818, 779, 757, 725, 694.  $^1\text{H}$  NMR  $\delta$ , ppm, J/Hz: 2.50 s ( $\text{CH}_3$ , 3H), 5.36 s ( $\text{CH}_2$ ), 7.16 d (1H, arom,  $J=8.2$  Hz), 7.62 dd (1H, arom,

$J=2.48$ , 8.46 Hz), 7.71 dd (1H, Im,  $J=1.78$ , 3.63 Hz), 7.75 dd (1H, arom,  $J=2.42$  Hz), 7.81 dd (1H, Im,  $J=1.78$ , 3.63 Hz), 9.29 s (1H, Im), 10.29 s (1H, CHO), 11.96 s (1H, OH).  $^{13}\text{C}$  NMR,  $\delta$ , ppm: 36.20, 51.45, 118.55, 122.62, 123.03, 124.45, 126.08, 129.13, 137.06, 161.86, 190.74. Elemental composition: formula  $\text{C}_{12}\text{H}_{13}\text{ClN}_2\text{O}_2$ . Found, %: C 56.89, H 4.11, N 10.96. Calculated, %: C 57.04, H 4.10, N 11.09.

For recent example of synthesis of (4) see [29].

#### 2.2.3. Synthesis of Schiff base (6) and its chloroferric derivative (8, Catalyst 1)

0.53 g (2 mmol) of 3-(3-formyl-4-hydroxybenzyl)-1-methyl-1H-imidazol-3-ium chloride (4) were dissolved in 10 mL of methanol. Then, 0.22 g (2 mmol) of benzylamine were added dropwise (5). The mixture was refluxed for 5 h, the solvent was partially removed under reduced pressure on a rotary evaporator, and the yellow product of (6) was precipitated by *n*-hexane. The 3-[(benzylimino) methyl]-4-hydroxybenzyl-1-methyl-1H-imidazol-3-ium chloride (6) was separated and washed with *n*-hexane and diethyl ether, and then it was dried at RT to give pale yellow oil. The reaction yield was 95%. IR  $\nu$ ,  $\text{cm}^{-1}$ : 3725, 3490, 3400, 3130, 3145, 3020, 3050, 2768, 2607, 2550, 2398, 2041, 1635, 1620, 1520, 1495, 1421, 1427, 1383, 1283, 1246, 1165, 1095, 1133, 1000, 935, 951, 845, 807, 759, 706, 676, 626, 580, 505.  $^1\text{H}$  NMR  $\delta$ , ppm, J/Hz: 3.86 s ( $\text{CH}_3$ , 3H), 4.43 s ( $\text{CH}_2$ ), 5.36 s ( $\text{CH}_2$ ), 6.92 d (1H, arom,  $J=8.8$  Hz), 7.20–7.39 m (5H, arom), 7.48 d (1H, arom,  $J=8.1$  Hz), 7.67 s (1H, arom), 7.73 s (1H, Im), 7.83 s (1H, Im), 9.36 s (1H, CH=N), 9.39 s (1H, Im), 13.63 s (1H, OH).  $^{13}\text{C}$  NMR,  $\delta$ , ppm: 15.62, 36.30, 51.68, 62.19, 65.39, 117.80, 118.68, 119.09, 122.57, 122.97, 124.36, 125.26, 126.07, 127.75, 128.34, 128.54, 128.81, 128.98, 129.10, 129.24, 129.45, 132.66, 133.54, 136.96, 138.88, 161.67, 161.86, 166.20. Elemental composition: formula  $\text{C}_{19}\text{H}_{20}\text{ClN}_3\text{O}_2$ . Found, %: C 66.58, H 5.93, N 12.13. Calculated, %: C 66.76, H 5.90, N 12.29.

A 50-mL, 2-necked, round-bottom flask was charged with a solution of chloride (6) (0.68 g, 2 mmol) in methanol (10 mL). To the yellow solution, 0.54 g (2 mmol) of  $\text{FeCl}_3 \cdot 6\text{H}_2\text{O}$  (7) was added and the solution turned into dark brown which was stirred for 5 h. Afterwards, the solvent was evaporated and the residue was washed with diethyl ether to give dark brown solid product. The dark brown solution was diluted with diethyl ether resulting in the precipitation of the dark brown solid product, which were filtered and washed with brine. The 3-[(benzylimino) methyl]-4-hydroxybenzyl-1-methyl-1H-imidazol-3-ium tetrachloroferrate(III) (8) was dried overnight under vacuum. The reaction yield was 94%.

The synthesis reaction of novel imidazolium-based iron-containing ionic substance is presented in Fig. 1.

For recent examples of synthesis the ionic metal complexes with both a Schiff base and imidazolium moiety see [30–32].

#### 2.2.4. Synthesis of magnetite and its chloroferric derivative (Catalyst 2)

$\text{Fe}_3\text{O}_4$  was synthesized by a co-precipitation method in a ferric to ferrous ion molar ratio of 2:1, in  $\text{NH}_4\text{OH}$ . The obtained magnetite was mixed with product (8) in the carrier fluid in the weight ratio 1:1.

### 2.3. Characterization methods

Nuclear magnetic resonance spectroscopy (NMR)  $^1\text{H}$  and  $^{13}\text{C}$  NMR spectra have been recorded for  $\text{CDCl}_3$  2% solution on a “Bruker Avance III” (400.13 and 100.61 MHz). Chemical shifts were reported in  $\delta$  values downfield from tetramethylsilane; Dimethyl sulfoxide ( $\text{DMSO}-d_6$ ) was used as a solvent.

Electrospray ionisation–mass spectrometry (ESI/MS) analyses were performed with an Agilent 6540 Q-TOF chromatograph

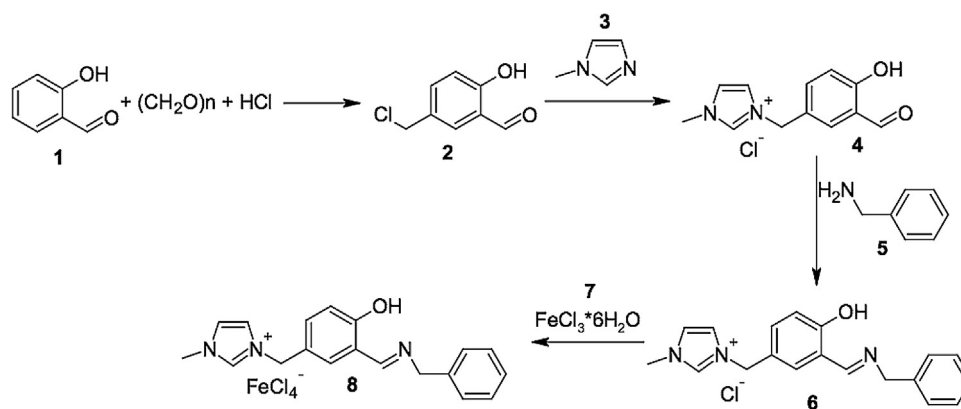


Fig. 1. Synthesis reaction of the catalysts.

equipped with an autosampler. The sample (in a concentration of approximately 10 ppm) was injected into the JetStream ESI ion source. MeOH was used as effluent solvent. The instrument was operated in the 4 GHz high resolution mode. Accurate mass measurement was achieved by constantly infusing a calibrant (masses: 121.0508 and 922.0098).

Differential scanning calorimetry (DSC) was performed with a computer-controlled Phoenix DSC 204 F1 thermal analyser (Netzsch, Selb, Germany) with argon as the protection gas. The samples were placed in aluminium pans which were cold-sealed under argon. Experimental data is displayed in such a way that exothermic peaks occur at negative heat flow and endothermic peaks at positive heat flow. DSC runs included heating and subsequent cooling at 5 °C/min. Given temperatures correspond to the onset of the respective thermal process.

A high-resolution scanning electron microscope (SEM) of type Supra 40 (Carl Zeiss, Oberkochen, Germany) equipped with a Schottky field emitter was employed to characterize the sample surface morphology down to the nanometer scale. The SEM was equipped with a large-area EDS (energy-dispersive X-ray spectrometer) detector of type Ultra Dry SDD (Silicon Drift Detector), from Thermo Fisher Scientific (Waltham, MA, USA). With this EDS system a semi-quantitative analysis of the elemental composition of the samples was carried out.

Infrared spectra of all samples were measured on a Jasco 660 Plus spectrometer in KBr disk, between 4000 and 400  $\text{cm}^{-1}$ , with a resolution of 4  $\text{cm}^{-1}$ .

The nitrogen adsorption and desorption isotherms, the Brunauer–Emmett–Teller (BET) tests were performed with a micromeritics ASAP 2020<sup>TM</sup> physisorption system (Norcross, USA) at 77 K. Interparticle space distribution was determined by the Barrett–Joyner–Halenda (BJH) method. Before analysis, the samples were degassed for 4 h at 105 °C under vacuum.

ESR detection of the photo-sensitized  $^1\text{O}_2$  was performed using an ESR spectrometer (MiniScope MS 300, Magnetech GmbH, Berlin, Germany) at a microwave power of 0.1 mW. The pollutant (5 mL) and 40 mM of 2,2,6,6-tetramethyl-4-piperidinol (TMP-OH) were transferred into a small dark vial and exposed to UVA ( $\lambda = 365 \text{ nm}$  from a UV spot light source lightingcure<sup>TM</sup>, model LC-8, from Hamamatsu Photonics, Germany).

#### 2.4. Kinetic experiments

Solutions containing the CBZ were prepared by adding an appropriate volume of stock solution to ultrapure water for the final concentration. The oxidation experiments, in absence of UVA light, were carried out on a rotator SB3 (VWR International, Germany),

whereas in the presence of UVA irradiation the experiments were conducted using an orbital shaker Heidolph Titramax 100 with continuous mixing. The initial pH of the micropollutant solution was 6.6 without any adjusting. Then a solution of 30%  $\text{H}_2\text{O}_2$  was added to achieve the selected  $\text{H}_2\text{O}_2$  concentrations, these being the basic conditions for the experiments. Samples of the reaction medium were withdrawn at regular intervals and filtered immediately through a 0.22  $\mu\text{m}$  Teflon membrane filter for HPLC analysis.

The photochemical experiments were performed using three parallel ordered UVA nm xenon lamps (ATLAS Material Testing Solution, Germany, 40  $\text{W m}^{-2}$ , photon flow in the UV range ( $290 \leq \lambda \leq 400 \text{ nm}$ ) of  $2.13 \times 10^{-7} \text{ Einstein s}^{-1}$ , measured by polychromatic actinometry with phenylglyoxylic acid in  $\text{AcN:H}_2\text{O} = 3:1$  (v/v)). The total reaction volume was 8 mL in all experiments; the irradiated surface area was 9.62  $\text{cm}^2$  and the irradiation pathlength 1.4 cm. Sample analysis of CBZ was performed by HPLC–MS/MS. A series 1100HPLC workstation (Agilent Technologies, Waldbronn, Germany) was coupled to an API 4500 TSQ triple stage quadrupole mass spectrometer (ABSciex, Darmstadt, Germany) (see SI). The relative standard deviation of three experiments was less than 4%.

### 3. Results and discussion

#### 3.1. Characterization

According to the micrographs provided by SEM as in Fig. 2 the structure of the Catalyst 1 is one of “intertwined platelets”, with sizes of several  $\mu\text{m}$  and about 100 nm thickness of the individual platelets. High-resolution images (see inset in Fig. 2 left) show a rather smooth platelet surface.

The morphology of the Catalyst 2 is defined by primary particles with sizes of about 100 nm and of a more or less “elongated” shape, see Fig. 2 right. A location on the sample where the shape of the primary nanoparticles is rather needle-like, of about 100–200 nm length and about 10 nm width is shown in the inset of Fig. 2 right.

In the EDX spectra of Catalyst 1 as in Fig. 3 (blue spectrum) Cl, Fe, C, N and O could be clearly identified—as expected from the chemical formula of the catalyst. No additional elements could be identified by EDX. Under the same conditions the EDX spectra of Catalyst 2 show Fe and O as the main constituent elements (confirming the presence of iron oxide) and Cl and C as minor elements, see Fig. 3. It should be noted that a reliable quantification of EDX spectra into atom-% is not possible for this type of samples. The strong (uneven) surface morphology leads to X-ray absorption which cannot be taken into account accurately in the available EDX quantification models.

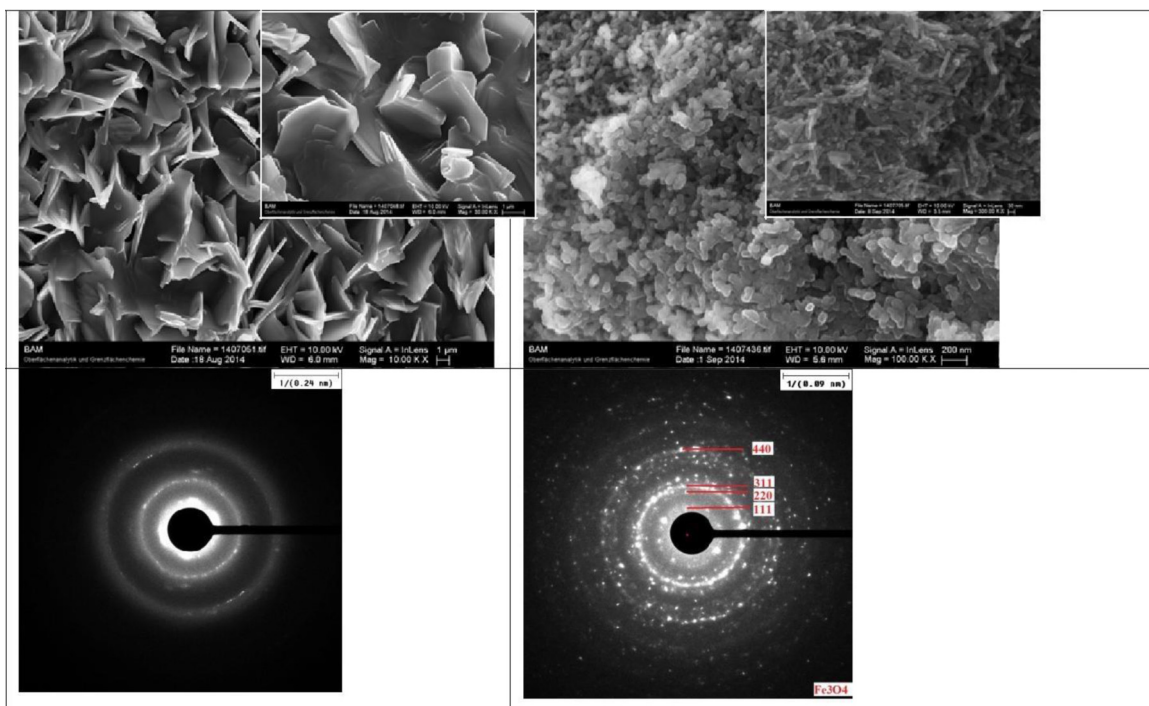


**Fig. 2.** (top) Representative SEM micrographs of the two catalysts: Catalyst 1 - left, the inset shows the sample at a higher magnification and Catalyst 2 - right, the inset shows a location on the sample where the shape of the primary particles is more prolonged (an acicular one); and (bottom) representative SAED patterns of the two catalysts taken at a TEM.

The SAED patterns of Catalyst 2 confirm the presence of magnetite.

Catalyst 1 structure has been confirmed through ESI–MS analysis (SI, Fig. S1). For this, the Catalyst 1 solution was electrodispersed into a thin aerosol. Ion  $m/z = 745.5165$  forms as a result of bond formation between two ligands of **8** with  $\text{FeCl}_3\text{OME}$ , water and MeOH. The peak  $M = 860.5843$  denotes the interaction of two ligands of **8**,  $\text{FeCl}_4^-$  and 3 water molecules. In the middle part of the spectrum, there is a peak with maximum intensity  $m/z = 519.3243$ , which could be formed as a result of MeOH cleavage at the decomposition of compound **8**·H<sub>2</sub>O according to the following pathway:  $\mathbf{8} \cdot \text{H}_2\text{O} + \text{CH}_3\text{O}^- = [\text{M}]^- + \text{CH}_3\text{OH}$ . The molecular ion is fragmented with intensive formation of ion radicals  $[\text{C}_6\text{H}_5\text{CH}_2\text{NH}_3]^+$ ,  $m/z = 108.163$  and a supramolecular ( $-\text{CH}=\text{NH}^+$ -protonated group) fragment  $[\mathbf{8} + \text{MeOH} + 4\text{H}_2\text{O}]^{2+}$ ,  $m/z = 198.23$  (experimental); 198.73 (calculated).

DSC results are presented in Fig. 4. During the first heating scan, a broad endothermic effect with the onset around 87.5 °C could be detected and can hence be classified as imidazolium-based iron-

containing ionic substance. No crystallization or glass transition peaks were detected within two heating-cooling cycles (Fig. 4).

A thorough analysis of IR spectra of the studied Catalyst 1 and Catalyst 2 permits identification of a group of absorption bands characteristic for the structure of the ligand part of the catalysts (Fig. 5).

It can be easily observed that presence of magnetite in Catalyst 2 influences the bond vibrations of the ligand. Thus, for example, a strong  $-\text{C}-\text{O}-$  stretching band at  $1155\text{ cm}^{-1}$  in the Catalyst 1 spectrum is shifted to higher frequencies ( $1158\text{ cm}^{-1}$ ) in the spectrum of Catalyst 2.

The peak at  $1271\text{ cm}^{-1}$  can be assigned to  $\text{C}-\text{N}$  bond stretching vibrations in the molecule of Catalyst 1. It disappears in the spectrum of Catalyst 2 most probably due to the shifting and overlapping with other vibrational bands. The peak at  $1612\text{ cm}^{-1}$  can be assigned to overlapping of  $\text{C}=\text{N}$  bond stretching vibrations with  $\text{C}=\text{C}$  stretching vibrations of the benzene ring in the Catalyst 1 spectrum being shifted to  $1623\text{ cm}^{-1}$ . The same benzene ring characteristic  $\text{C}-\text{H}$  vibrations at  $696$  and  $745\text{ cm}^{-1}$  appearing in the

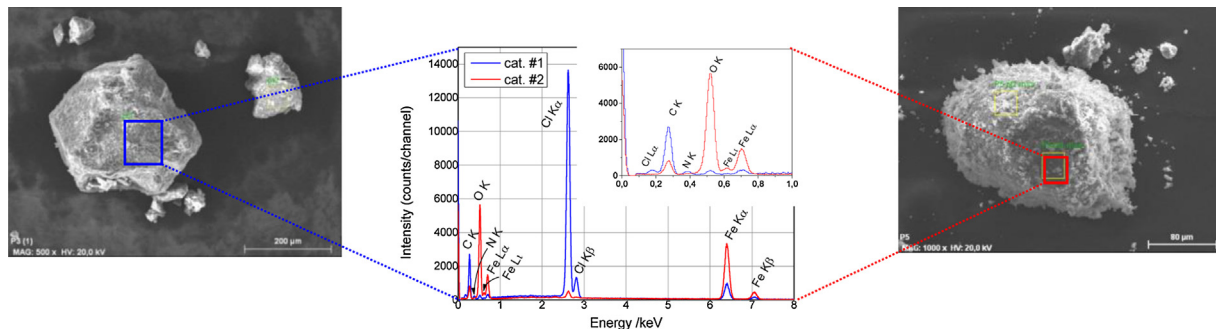


**Fig. 3.** 20 kV EDX spectra of the two catalysts together with SEM micrographs illustrating the locations where the spectra have been taken. The inset in the plot containing the EDX spectra is a detail in the 0–1 keV spectral range.

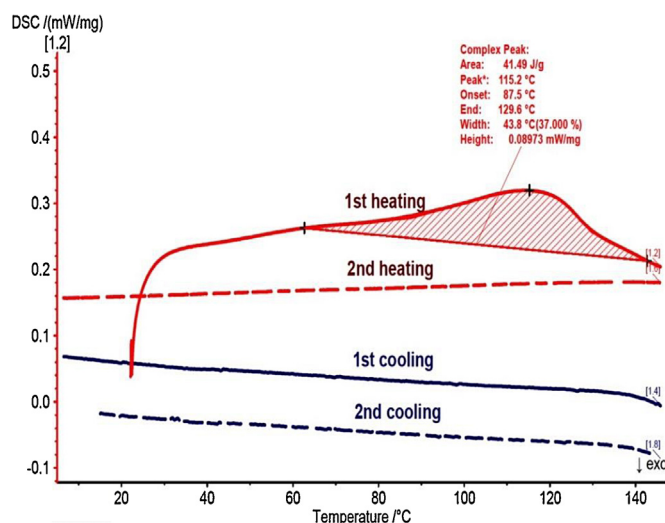


Fig. 4. DSC curves measured with heating and cooling rates of  $5^{\circ}\text{C min}^{-1}$  on the sample of 8.

spectrum of *Catalyst 1*, appear overlapped with a new band with a peak at  $796\text{ cm}^{-1}$  in the spectrum of *Catalyst 2*.

Several overlapped peaks in the region of  $3050\text{--}2850\text{ cm}^{-1}$  of both spectra represent overlapped characteristic  $\text{C--H}$  vibrations of the methyl, methylene group, and imidazolium ring. As well as in the case of other characteristic bands, shifts are observed in the spectrum of *Catalyst 2*.  $\sigma_{\text{OH}}$  broad band with a peak at  $3447\text{ cm}^{-1}$  in the *Catalyst 1* spectrum is shifted to lower wave numbers ( $3418\text{ cm}^{-1}$ ) in the spectrum of *Catalyst 2*.

A band at  $618.07\text{ cm}^{-1}$  can be assigned to the  $\text{Fe--O}$  vibrations in *Catalyst 1* and its intensity is significantly increased with a slight shift to higher energies, i.e. to higher wavenumbers, in the spectrum of *Catalyst 2* due to the presence of magnetite.

From all the observations above it is easy to suggest that the largest shifts in the vibrations of the groups involved in coordinative or ion binding with iron (III) of the catalyst molecule in the spectra of *Catalyst 2* appear due to the presence of magnetite.

We have also investigated the property as a photosensitizer of the  $\text{Fe(III)}$ -based IL to generate singlet oxygen. The formation and quenching of the photosensitized singlet molecular oxygen,  $^1\text{O}_2$ , generated by the catalyst, was investigated by ESR using 2,2,6,6-tetramethyl-4-piperidinol (TMP-OH) as spin trap. Fig. 6 shows the ESR spectra obtained from the samples containing TMP-OH in the presence of catalyst (a) and in its absence (b). This ESR spectrum consists of three equidistant and equi-intense hyperfine lines.

Singlet molecular oxygen ( $\text{O}_2(^1\Delta_g)$ , denoted throughout as  $^1\text{O}_2$ ), the lowest electronic excited state of molecular oxygen, is an important oxidizing species in chemical processes and one of the main activated species responsible for the damaging effects of light on biological systems (photodynamic effects) [6]. This activated metastable state is much more reactive than the ground triplet state ( $\text{O}_2(^3\Sigma_g)$ , denoted throughout as  $^3\text{O}_2$ ) and has been attracting interest in both practical and fundamental aspects. Photosensitization is primarily responsible for the production of  $^1\text{O}_2$  [33]. This process can be summarized as follows: a sensitizer is promoted by the absorption of a photon to an electronically excited singlet state and can subsequently undergo intersystem crossing to generate a longer lived excited triplet state. Singlet oxygen may be then produced by energy transfer to dissolved molecular oxygen [33,34].

Fig. 6b shows the samples containing only TMP-OH exposed to UV illumination for 90 min. In contrast, after a 90-min exposure to UV light, the solution containing the catalyst as well as the control solution (containing only TMP-OH), showed a characteristic ESR signal (Fig. 6a).

The signal intensity of the 4-hydroxy-2,2,6,6-tetramethylpiperidine-1-oxyl (TEMPOL) spectra acquired for the catalyst is larger than for the control solution. This suggests that, under exposure to UV light, the catalyst contributed to the overall singlet oxygen formation. The ESR experiments point to an efficient formation of  $^1\text{O}_2$  by the studied catalyst in aqueous suspension. In the presence of the *Catalyst 1*  $55\text{ }\mu\text{M}$  of  $^1\text{O}_2$  was generated after 90 min of UVA irradiation (Table 1).

### 3.2. Catalytic and photocatalytic activity

The effects of the catalyst load, pH,  $\text{H}_2\text{O}_2$  concentration and UVA light were also investigated (Fig. 7).

The degradation of pollutant in the dark was found to be negligible. The reactivity of the two catalysts on pollutant removal was studied at room temperature by using solutions with pH values determined initially. After 30 min of catalytic oxidation with a dose of  $1.0\text{ g/L}$  of catalysts the removal was higher than 30% at pH 6.6, see Fig. 7a. The maximum conversion of CBZ over 73% was achieved after 120 min from the start of the reaction for *Catalyst 1*. Significantly lower efficiency of 50% for CBZ degradation was observed over *Catalyst 2* at the same pH. Both catalysts showed lower removal rates at alkaline pH. By further increasing the amount of catalyst to  $1.5\text{ g/L}$ , an increase of the pollutant removals of 9% for *Catalyst 2* and 16% for *Catalyst 1*, respectively, were observed, see Fig. 7b. We selected the concentration of  $1.0\text{ g/L}$  of catalysts and pH 6.6 for our further experiments. Although the classical Fenton process offers a cost effective source of hydroxyl radicals, the major drawback

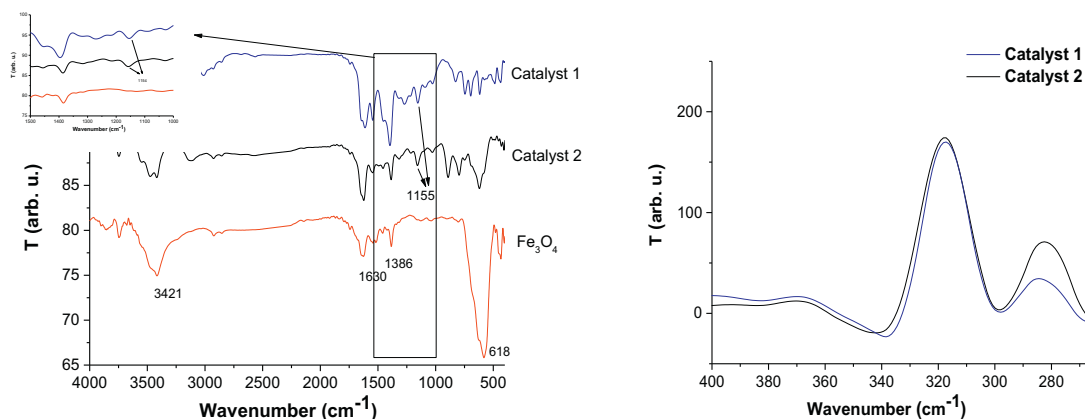
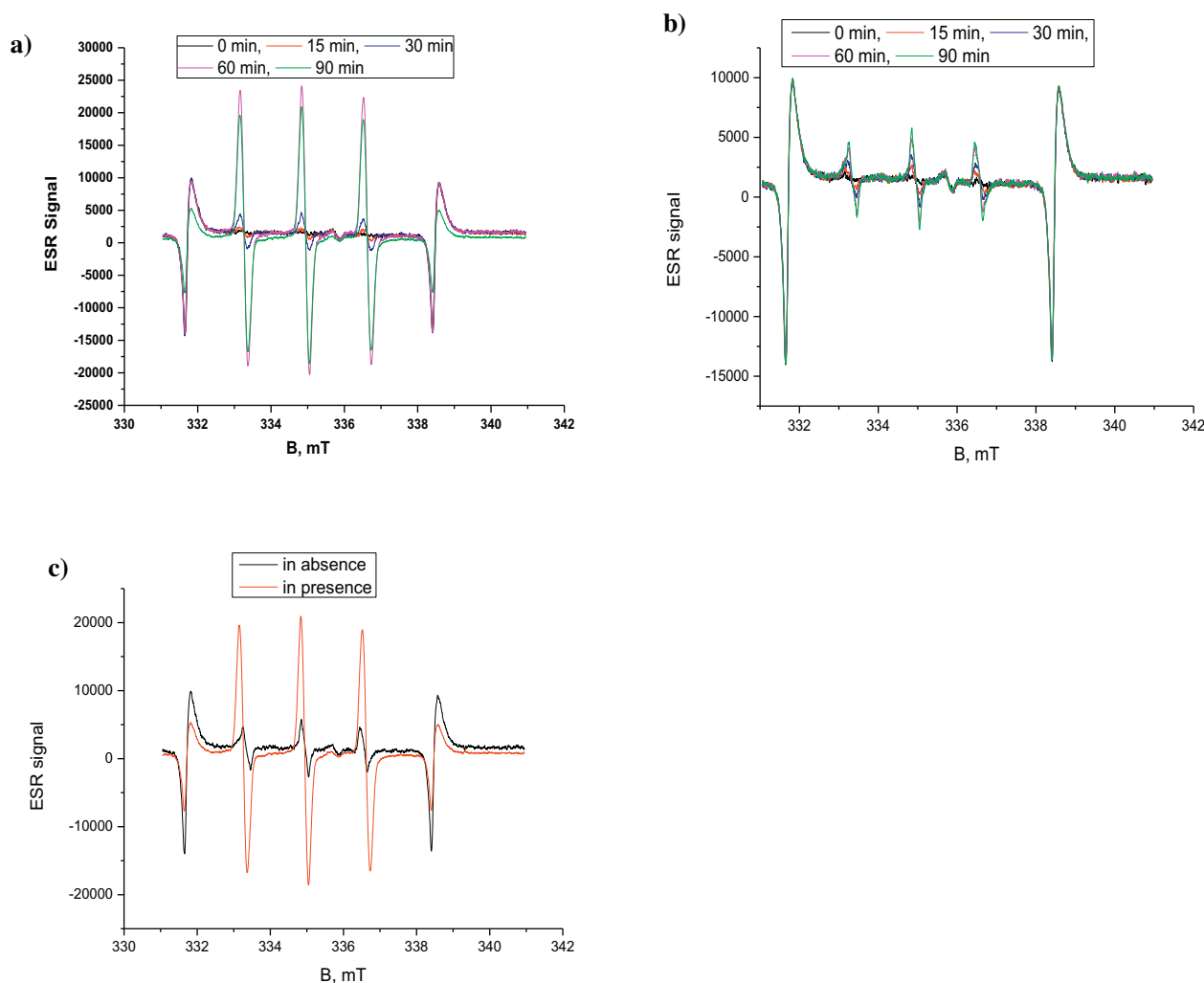


Fig. 5. FTIR spectra of the two catalysts and magnetite.



**Fig. 6.** The ESR spectra of TEMPOL acquired sequentially during 90 min of UV illumination ( $\lambda = 365$  nm) of a TMP-OH solution in the presence of the catalyst (a) and of a control solution (b). The direct comparison after 90 min of reaction with/without catalyst is presented in (c).

that limits the industrial application of this technology is the tight range of pH (3–4) in which the reaction proceeds. From the practical point of view, nearly neutral pH is important. A solution for this problem could be the use of heterogeneous solid Fenton catalysts, such as catalysts presented in our study. Moreover, one feature of these catalysts is the facile separation. The catalysts can be simply separated by decantation from the reaction mixture [25,28,35], regenerated with deionized water and reused for several times.

In the next experiments, the effect of different hydrogen peroxide concentrations was studied using the same operational

conditions: pH 6.6,  $t = 25^\circ\text{C}$  and 1.0 g/L of catalyst. The results are presented in Fig. 7c.

As expected, addition of hydrogen peroxide accelerated the removal of the pollutant. This can be explained by the effect of the  $\text{OH}^\bullet$  radicals produced additionally. After 15 min of reaction time at a dose of  $200\ \mu\text{M}$   $\text{H}_2\text{O}_2$ , 29% of CBZ removal was achieved over 1.0 g/L of Catalyst 2, whereas over Catalyst 1 over 77% of the pollutant was removed. Increasing the hydrogen peroxide concentration to a value of 10 mM slightly accelerated the reaction, after the same reaction time 40% of CBZ was removed over Catalyst 2 and completely degraded over Catalyst 1.

**Table 1**

Evolution of the  $^1\text{O}_2$  concentration ( $\mu\text{M}$ ) over the reaction time.

Time, min	CBZ + TEMP + Catalyst 1 + UV	TEMP + Catalyst 1 + UV	TEMP + UV	CBZ + TEMP + UV	Rose bengal + TEMP + UV
5	0.13	0.13	n.d.	0.10	3.93
10	0.31	0.16	0.00	0.16	11.45
15	0.40	0.29	0.00	0.23	17.40
20	0.76	0.54	0.00	0.00	20.84
25	0.86	0.61	0.00	0.00	23.78
30	6.20	0.93	0.00	0.54	27.03
45	35.16	16.40	n.d.	n.d.	31.57
50	46.45	19.83	n.d.	n.d.	n.d.
60	55.58	34.14	0.97	1.11	n.d.
70	55.49	47.97	n.d.	n.d.	n.d.
90	n.d.	55.34	1.20	1.19	n.d.

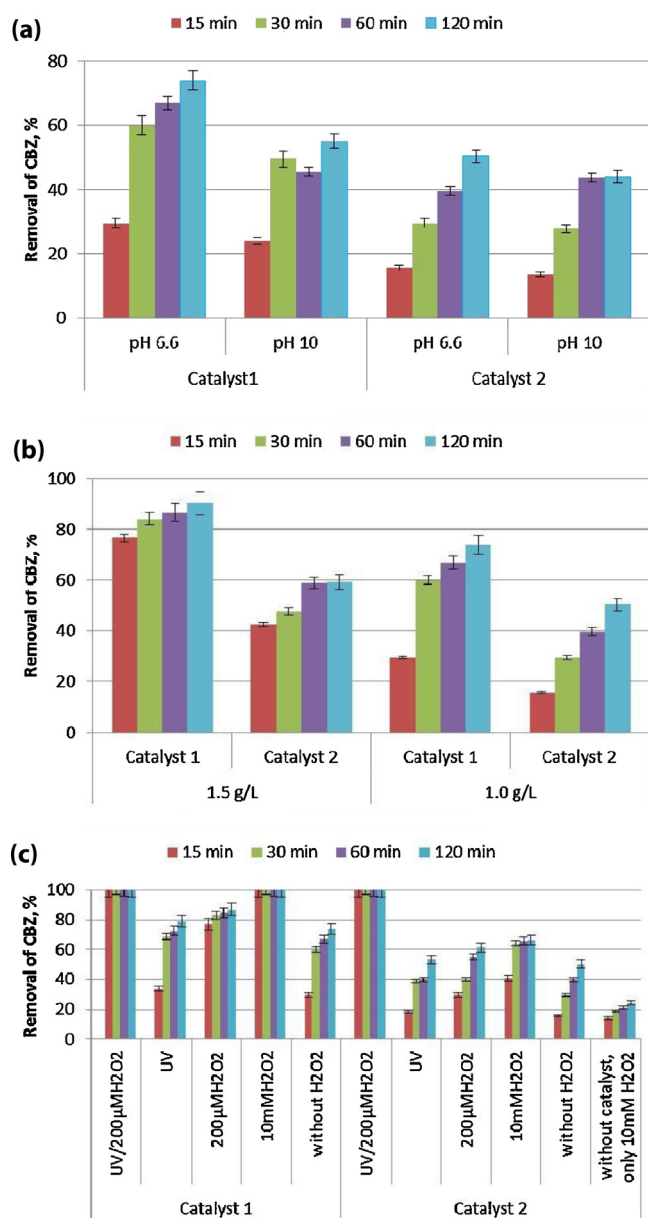


Fig. 7. Effect of pH (a), catalyst dosage (b), H<sub>2</sub>O<sub>2</sub> concentration and UV light (c). Initial conditions: 0.5 μM of CBZ, 25 °C.

The effect of UV light on the degradation of CBZ was also investigated (Fig. 7c). From a practical standpoint, due to the cost of H<sub>2</sub>O<sub>2</sub>, we have selected the concentration of 200 μM H<sub>2</sub>O<sub>2</sub> as the optimal concentration for these experiments. After 30 min of irradiation in the absence of H<sub>2</sub>O<sub>2</sub>, the CBZ removal rate in MilliQ water was only 39% over Catalyst 2 and 68% over Catalyst 1. At the same reaction time, by adding 200 μM H<sub>2</sub>O<sub>2</sub>, CBZ was completely removed over both catalysts. In all experimental conditions, Catalyst 1 showed enhanced activity. The measured BET specific surface area of the paramagnetic form (Catalyst 2) of 21.53 m<sup>2</sup>/g is significantly higher than that of Catalyst 1 of 2.19 m<sup>2</sup>/g (as indicated also by the SEM micrographs, see Fig. 2). This suggests that the different reactivity of the catalysts is not attributed to the surface area, but to the iron ions, i.e. the FeCl<sub>4</sub><sup>−</sup> anion (higher for Catalyst 1) that could activate molecular oxygen via a single-electron reduction pathway producing reactive oxygen species (ROS) and subsequently reducing the pollutants. The increased fraction of FeCl<sub>3</sub> leads to a stronger Lewis acid-base of the FeCl<sub>3</sub>-based IL [28] and thus accelerate electron

transfer reactions. Our results on singlet oxygen formation support this assumption. Similar results were reported for oxidative desulfurization of fuels, oxidation of aromatic alcohols and benzylation of arenes [25,28,35].

Lower removal rates (~12%) have been reported by Sun et al. [36] for the removal of CBZ over pure magnetite in aqueous solution in the presence of much higher hydrogen peroxide concentration (600 mM, 1.84 g/L nano-Fe<sub>3</sub>O<sub>4</sub>, reaction time 1 h). Compared with the data reported in the literature [37] using FeCl<sub>3</sub> as a catalyst and a concentration of CBZ (0.423 μM) comparable to that used in our study, the removal of CBZ was less than 18% using much higher concentration of H<sub>2</sub>O<sub>2</sub> (2.78 mM) and 19.7% under UV irradiation at the same concentration of hydrogen peroxide after 300 min of reaction time. Moreover, it is well known that FeCl<sub>3</sub> is highly corrosive and easily deliquescent, but these catalysts are not [25].

As proposed by several authors, e.g. [38], and in our earlier studies [5,6], the formation of oxidation intermediates of CBZ can be directly attributed to the attack of ROS resulting in the hydroxylation of either the double bond or the aromatic rings of CBZ. Additionally, an alternative pathway is the attack of •OH on the central seven-membered ring of CBZ to form 10,11-epoxy-CBZ [38b]. The mechanism might involve an intramolecular reaction, with H<sub>2</sub>O loss arising from a transient dihydroxy-CBZ radical and/or quinoid-CBZ [38,39]. Furthermore, an oxidative ring-cleavage by hydroxyl radical attack leads to aliphatic compound formation, such as HCOOH, CH<sub>3</sub>COOH, and CH<sub>3</sub>CHO, and, finally, to CO<sub>2</sub> [5,39]. A more recent work presents in detail the mechanism and the toxicity of the resulting effluents for the oxidation of CBZ [39].

#### 4. Conclusions

In this study a new Fe-based highly active ionic liquid containing an imidazolium salt and a Schiff base and its paramagnetic form have been synthesized, characterized and evaluated as catalysts for removal of CBZ. The morphological structure of the Catalyst 1 is one of “intertwined platelets”, with sizes of several μm and about 100 nm thickness of the individual platelets, whereas the structure of the Catalyst 2 is defined by primary particles with sizes of about 100 nm and of a more or less “stretched” shape. High-resolution SEM images show a rather smooth platelet surface. In the EDX spectra of Catalyst 1 Cl, Fe, C, N and O could be clearly identified. Under the same conditions the EDX spectra of Catalyst 2 show Fe and O as the main constituent elements (confirming the presence of iron oxide) and Cl and C as minor elements. The chemical structure of Catalyst 1 has been confirmed through ESI-MS, FTIR and DSC analyses. The ESR experiments point to an efficient formation of <sup>1</sup>O<sub>2</sub> by the studied catalyst in aqueous suspension. About 55 times more <sup>1</sup>O<sub>2</sub> was generated in the presence of the catalyst than in its absence. After 15 min of reaction time at a dose of 200 μM H<sub>2</sub>O<sub>2</sub>, 29% of CBZ removal was achieved over 1.0 g/L of Catalyst 2, whereas over the same concentration of Catalyst 1 over 77% of the pollutant was removed. At the same reaction time, in the presence of UVA irradiation and 200 μM H<sub>2</sub>O<sub>2</sub>, CBZ was completely removed over both catalysts. Thus, it could be demonstrated that the developed ionic liquid catalysts are promising photocatalysts, e.g. for the removal of micropollutants from contaminated wastewater.

#### Acknowledgements

The authors acknowledge the financial support of the Romanian Ministry of National Education CNCS-UEFISCDI through the national grant type PN-II -ID-PCE-2012-4-0477 and BAM Federal Institute for Materials Research and Testing; the authors also thank Dr. D. Prodius from the Institute of Chemistry, Academy of Sci-

ences of Moldova for helpful discussion and Prof. Dr. A. Pui (FTIR recordings) from 'Alexandru Ioan Cuza' University in Iasi, Romania.

## Appendix A. Supplementary data

Supplementary data associated with this article can be found, in the online version, at <http://dx.doi.org/10.1016/j.apcatb.2015.10.032>.

## References

- [1] B. Morasch, F. Bonvin, H. Reiser, D. Grandjean, L.F. de Alencastro, C. Perazzolo, N. Chevre, T. Kohn, *Environ. Toxicol. Chem.* 29 (8) (2010) 1658–1668.
- [2] R.L. Oulton, T. Kohn, D.M. Cwierny, *J. Environ. Monit.* 12 (11) (2010) 1956–1978.
- [3] F. Bonvin, R. Rutler, N. Chevre, J. Halder, T. Kohn, *Environ. Sci. Technol.* 45 (2011) 4702–4709.
- [4] B. Escher, R. Baumgartner, M. Koller, K. Treyer, J. Lienert, C.S. McArdell, *Water Res.* 45 (2011) 75–92.
- [5] M. Neamțu, D. Grandjean, A. Sienkiewicz, S. Le Faucheur, V. Slaveykova, J. Velez Colmenares, C. Pulgarín, F.L. de Alencastro, *Appl. Catal. B* 158–159 (2014) 30–37.
- [6] C. Nadejde, M. Neamțu, V.-D. Hodoroaba, R.J. Schneider, A. Paul, G. Ababei, U. Panne, *Appl. Catal. B* 176 (2015) 667–677.
- [7] C.G. Daughton, T.A. Ternes, *Environ. Health Perspect.* 107 (6) (1999) 907–938.
- [8] G. Duca, V. Boldescu, *Pharmaceuticals and personal care products in the environment. The role of ecological chemistry in pollution research and sustainable development*, in: A.M. Bahadır, G. Duca (Eds.), In NATO Science for Peace and Security Series, Sub-Series C. Environmental Security, Springer, 2009, pp. 27–35.
- [9] A. Bahlmann, J.J. Carvalho, M.G. Weller, U. Panne, R.J. Schneider, *Chemosphere* 89 (2012) 1278–1286.
- [10] M. Clara, B. Strenn, N. Kreuzinger, *Water Res.* 38 (4) (2004) 947–954.
- [11] L. Martin-Diaz, S. Franzellitti, S. Buratti, P. Valbonesi, A. Capuzzo, E. Fabbri, *Aquat. Toxicol.* 94 (3) (2009) 177–185.
- [12] G. Vernouillet, P. Eullaffroy, A. Lajeunesse, C. Blaise, F. Gagné, P. Juneau, *Chemosphere* 80 (9) (2010) 1062–1068.
- [13] V. Contardo-Jara, C. Lorenz, S. Pflugmacher, G. Nützmann, W. Kloas, C. Wiegand, *Aquat. Toxicol.* 105 (3–4) (2011) 428–437.
- [14] R. Freitas, Â. Almeida, V. Calisto, C. Velez, A. Moreira, R.J. Schneider, V.I. Esteves, F.J. Wrona, A.M.V.M. Soares, E. Figueira, *Environ. Pollut.* 202 (2015) 205–214.
- [15] D. Donner, T. Kosjek, S. Qualmann, K. Ole Kusk, E. Heath, E.M. Revitt, A. Ledin, H. Rasmus Andersen, *Sci. Total Environ.* 443 (2013) 870–876.
- [16] L. Haroune, M. Salaun, A. Ménard, C.Y. Legault, J.P. Bellenger, *Sci. Total Environ.* 475 (2014) 16–22.
- [17] (a) A. Dhakshinamoorthy, S. Navalón, M. Alvaro, H. Garcia, *ChemSusChem* 5 (2012) 46–64;  
(b) P.V. Nidheesh, *RSC Adv.* 5 (2015) 40552–40577.
- [18] (a) X. Li, J. Wang, A.I. Rykov, V.K. Sharma, H. Wei, C. Jin, X. Liu, M. Li, S. Yu, C. Sun, D.D. Dionysiou, *Catal. Sci. Technol.* 5 (2015) 504–514;  
(b) B. Qiu, M. Xing, J. Zhang, J. Mater. Chem. A 3 (2015) 12820–12827.
- [19] J.P. Hallett, T. Welton, *Chem. Rev.* 111 (5) (2011) 3508–3576.
- [20] M. Galiński, A. Lewandowski, I. Stępnik, *Electrochim. Acta* 51 (26) (2006) 5567–5580.
- [21] S.Y. Lee, A. Ogawa, M. Kanno, H. Nakamoto, T. Yasuda, M. Watanabe, *J. Am. Chem. Soc.* 132 (28) (2010) 9764–9773.
- [22] M.D. Bermúdez, A.E. Jiménez, J. Sanes, F.J. Carrión, *Molecules* 14 (8) (2009) 2888–2908.
- [23] (a) D. Prodius, F. Macaev, E. Stingaci, V. Pogrebnoi, V. Mereacre, G. Novitchi, G.E. Kostakis, C.E. Anson, A.K. Powell, *Chem. Commun.* 49 (2013) 1915–1917;  
(b) J. Estager, J.D. Holbrey, M. Swadźba-Kwaśny, *Chem. Soc. Rev.* 43 (2014) 847–886.
- [24] L. Fischer, T. Falta, G. Köllensperger, A. Stojanovic, D. Kogelnig, M. Galanski, R. Krachler, B.K. Keppler, S. Hann, *Water Res.* 45 (15) (2011) 4601–4614.
- [25] W. Jiang, W. Zhu, H. Li, J. Xiong, S. Xun, Zh. Zhao, *RSC Adv.* 3 (2013) 2355–2361.
- [26] W. Zhu, W. Huang, H. Li, M. Zhang, W. Jiang, G. Chen, C. Han, *Fuel Process. Technol.* 92 (10) (2011) 1842–1848.
- [27] P.S. Kulkarni, L.A. Neves, I.M. Coelho, C.A. Afonso, J.G. Crespo, *Environ. Sci. Technol.* 46 (1) (2011) 462–468.
- [28] J. Gao, J.Q. Wang, Q.W. Song, L.N. He, *Green Chem.* 13 (5) (2011) 1182–1186.
- [29] R.D. Singer, P. U. Naik, *Ionic liquids compressing ligands containing positively charged heterocyclic ring useful as catalyst and for metal extractions*. Patent WO 2009/105881 A1.
- [30] R. Zhong, Y.-N. Wang, X.-Q. Guo, Z.-X. Chen, X.-F. Hou, *Chem. Eur. J.* 17 (2011) 11041–11051.
- [31] R.I. Kureshy, K.J. Prathap, T. Roy, N.Ch. Maity, N.H. Khan, S.H.R. Abdi, H.C. Bajaj, *Adv. Synth. Catal.* 352 (2010) 3053–3060.
- [32] P.U. Naik, G.J. McManus, M.J. Zaworotko, Robert D. Singer, *Dalton Trans.* 36 (2008) 4834–4836.
- [33] A.H. Thomas, C. Lorente, A.L. Capparelli, C.G. Martínez, A.M. Braun, E. Oliveros, *Photochem. Photobiol. Sci.* 2 (2003) 245–250.
- [34] A.M. Braun, M.T. Maurette, E. Oliveros, *Photochemical Technology*, Translated by D. Ollis and N. Serpone, Wiley, Chichester, 1991.
- [35] C.X. Miao, J.-Q. Wang, B. Yu, W.G. Cheng, J. Sun, S. Chanfreau, L.N. He, S.-J. Zhang, *Chem. Commun.* 47 (2011) 2697–2699.
- [36] S.-P. Sun, X. Zeng, C. Li, A.T. Lemley, *J. Mol. Catal. A: Chem.* 371 (2013) 94–103.
- [37] N. Klamerth, L. Rizzo, S. Malato, M.I. Maldonado, A. Aguilera, A.R. Fernández-Alba, *Water Res.* 44 (2010) 545–554.
- [38] (a) S.-P. Sun, X. Zeng, C. Li, A.T. Lemley, *J. Hazard. Mater.* 252–253 (2013) 155–165;  
(b) C. Martínez, M.L. Canle, M.I. Fernández, J.A. Santaballa, J. Faria, *Appl. Catal. B* 102 (2011) 563–571;  
(c) A. Ghauch, H. Baydoun, P. Dermesropian, *Chem. Eng. J.* 172 (2011) 18–27;  
(d) S. Chiron, C. Minero, D. Vione, *Environ. Sci. Technol.* 40 (2006) 5977–5983.
- [39] V.M. Monsalvo, J. Lopez, M. Munoz, Z.M. de Pedro, J.A. Casas, A.F. Mohedano, J.J. Rodriguez, *Chem. Eng. J.* 264 (2015) 856–862.